A Shifted Frequency Impedance Model of Doubly Fed Induction Generator (DFIG)-Based Wind Farms and Its Applications on S^{2}SI Analysis

Fan Shi, *Student Member, IEEE*, Dewu Shu, *Member, IEEE*, Zheng Yan, *Member, IEEE*, and Zhao Song

***Abstract*—The emerging sub-/super-synchronous interactions (S2SI) related stability issues caused by the interactions of doubly fed induction generator (DFIG)-based wind farms and the large-scale ac grids have aroused great concerns. For this particular issue, this article is aimed to fill the gap and propose new time-domain and phasor-domain sub-/super-synchronous impedance models (S2SIM), primarily to disclaim the electro-magnetic stability of the S2SI phenomena. First, the unified *dq* frame impedance model of the DFIGs have been proposed, including the individual and interactive impact of every control sections, such as the induction machine, the grid-side converter, the rotor-side converter, and the outer dc voltage controller, etc. Then, the more general time-domain S2SIM and phasor-domain shifted frequency S2SIM (SF-S2SIM) have been derived to reveal the electro-magnetic stability mechanism, especially aroused by S2SI. Next, the relationships between S2SIM/SF-S2SIM and the *dq*/sequence impedance models have been developed based on matrix transformation and the frequency shifting techniques. Finally, the electro-magnetic stability of the practical DFIG-based wind farms, associated with large-scale ac grids in China, have been well evaluated by the proposed S2SIM/SF-S2SIM based electro-magnetic stability method.**

***Index Terms*—Electro-magnetic stability, sub-/super-synchronous interaction (S2SI), sub-/super-synchronous impedance model (S2SIM), shifted phasor based S2SIM, overall impedance model.**

I. Introduction

With the high-level penetration of the wind power, the wide frequency band interactions between the wind turbines and the ac grids become more severe [1]–[3]. As a result, different types of wide frequency band oscillation phenomena have appeared, such as the subsynchronous resonance (SSR) [4]–[5], subsynchronous control interaction (SSCI) [6]–[8], or super-low frequency oscillations between large-scale wind farms and ac grids [9], etc. Although the SSR issues have been studied for decades, unluckily, the new emerging sub-/super-synchronous oscillation (S2SO) aroused by wide frequency band interactions between converters and large-scale ac grids has been detected worldwide, for instance, the 2.5 Hz/97.5 Hz sub-/super-synchronous interaction (S2SI) event in China southern grid [10], the 8.1/91.9 Hz oscillation event aroused by wide frequency band interactions between doubly fed induction generator (DFIG)-based wind farms and large-scale ac grids [11], etc. As the mechanism and the influencing factors of the S2SI phenomena is quite different from the traditional SSR event, many effects from both academic and industrial communities have been made to evaluate the electromagnetic stability of the S2SI phenomena, where typical methods include the eigenvalue analysis method and the impedance analysis method. As the eigenvalue analysis method suffers from typical drawbacks, such as, the requirement of every detailed structure of the whole system, in-availability to deal with the black or grey box, etc., the impedance analysis method is recommended. This is because the overall electro-magnetic stability can be evaluated where each component can be modeled as an impedance (matrix) in an independent and separated way. Consequently, the system stability can be analyzed by the impedance ratio of the converter and the ac grid according to the generalized Nyquist criterion (GNC) [12], [13].

Admittedly, the impedance analysis method has been widely adopted to study the electro-magnetic stability of two-level voltage source converter (VSC) related systems, where the key issue is how to deal with the nonlinearity aroused by the inner current controllers and the phase-locked loop (PLL). Regarding the VSC impedance modeling, there are two main methods: the harmonic linearization method in the phase domain [14] and the typical linearization method in *dq* domain [15], resulting in the corresponding sequence impedance and *dq* impedance models. It is noted that both of *dq* and sequence impedance models are characterized as two-by-two matrices, where it thus gives rise to a concern on how to interpret nonzero nondiagonal terms and what are their consequences on stability. In this regard, recent modeling works, a complex transfer function based (e.g., [18] and [19]), a modified sequence domain method [20] have been proposed to considering the impact of the PLL in great details.

The above-mentioned methods are applicable for wind turbine systems, however, the induction machine (IM) or the permanent magnet synchronous machine models will complicate the overall

Manuscript received December 6, 2019; revised March 10, 2020; accepted May 23, 2020. Date of publication May 31, 2020; date of current version September 4, 2020. This work was supported in part by the Shanghai Sailing Program under Grant 19YF1423500, and in part by the Shanghai Jiao Tong University Scientific and Technological Innovation Funds, National Key Research and Development Program of China under Grant 2019YFE0102900. Recommended for publication by Associate Editor B. G. Fernandes. *(Corresponding author: Dewu Shu.)*

The authors are with the High-Performance Simulation Center, Key Lab of Control and Power Transmission and Conversion, Department of Electrical Engineering, Shanghai Jiaotong University, Shanghai 200240, China (e-mail: jwnl.hbfl@sjtu.edu.cn; shudewu@sjtu.edu.cn; yanz@sjtu.edu.cn; yanz@sjtu.edu.cn).

Color versions of one or more of the figures in this article are available online at http://ieeexplore.ieee.org.

Digital Object Identifier 10.1109/TPEL.2020.2999113

dq or sequence models of wind farms, especially the more complicated impedance models of DFIG-based wind farms. Up to now, impedance models of wind farms have only been proposed where are parts are simplified based on the model reduction technique. For example, in [2], [21], and [22], the impedance model of a single grid-side converter (GSC) or rotor-side converter (RSC) is given for the type IV wind turbine, where the other is simplified as a constant power load. Concerning the type III wind turbine, which is the focus of our manuscript, the dc voltage of the converter is usually assumed constant so that the GSC and RSC are modeled in a separate way [1]. Concerning the impedance model of the type III or the DFIG-based wind farms, especially associated with the S2SI phenomena, there are still some tricky issues are required to be resolved: 1) the traditional *dq* or sequence impedance model is mainly concerned with undesirable disturbances in *dq* or sequence axis. The impedance model, which is primarily associated with the S2SI phenomena, should be proposed to study the mechanism of S2SI related stability issues; 2) the overall S2SI related impedance model, incorporating the interactive impact between the GSC and the RSC should be given, considering the overall and individual impact of the outer dc voltage controller, the inner current controller, and the PLL, etc. In other words, in what frequency band, different control sections will reshape the overall impedance model; 3) the relationships between the S2SI related impedance model and the traditional *dq*/sequence impedance models should be revealed.

In order to reveal the electro-magnetic stability of the DFIG based farms associated with the S2SI related issues, the overall *dq* impedance model of the DFIG is proposed, including the impact of the IM, the GSC, the RSC, and the outer dc voltage controller, etc. More importantly, the more general time-domain sub-/super-synchronous impedance model (S2SIM) and phasor-domain shifted frequency S2SIM (SF-S2SIM) have been derived. The contributions of this work are given as follows.

1) The overall *dq* impedance model of the DFIG-based wind farms have been derived, incorporating the individual and interactive impact of every control sections, such as the IM, the GSC, the RSC, and the outer dc voltage controller, etc.
2) The more general time-domain S2SIM and phasor-domain shifted frequency S2SIM (SF-S2SIM) have been derived to reveal the electro-magnetic stability mechanism aroused by S2SI.
3) The relationships between S2SIM/SF-S2SIM and the traditional *dq*/sequence impedance models have been developed based on matrix transformation and the frequency shifting techniques;
4) The S2SIM/SF-S2SIM based electro-magnetic stability method have been constructed and evaluated.

The rest of this article is organized as follows. Section II introduces the unified *dq*-frame frequency coupled impedance for the DFIGs. In Section III, the S2SIM and the SF-S2SIM have been proposed, where the relationships between S2SIM/SF-S2SIM and *dq*/sequence impedance models will be further revealed; Section V examines the performance of the proposed method on a practical large-scale DFIG-based wind farms and ac grids in China. Finally, Section V concludes this article.

II. Unified *DQ*-Frame Frequency Coupled Impedance Model for the DFIGs

In order to study the electro-magnetic stability aroused by wide frequency interactions between large-scale DFIG-based wind farms and the ac grids, the unified *dq*-frame frequency coupled impedance model for the DFIGs is proposed, including the IM model, RSC (includes an inner loop current controller), GSC (includes an inner loop current controller), dc link (includes the dc voltage controller) and the synchronous reference frame PLL (SRF-PLL). Here, the RSC takes the role of injecting active current while the GSC is responsible for maintaining dc-bus voltage. Stator-voltage oriented vector-control based on PLL, without loss of generality, is utilized for the decoupled control between *d*- and *q*-axis currents.

Previous research has revealed that the current controllers of the RSC and GSC are more related to the high frequency or medium frequency band of the DFIGs, while the outer dc voltage controller of the GSC is more related to the low frequency dynamics [25]. It is an important issue that which parts of the DFIG contribute to the overall impedance model of the DFIG more significantly than others. To study the impact of different parts of the DFIG on the overall *dq* frame based impedance model, five types of DFIG impedance models are detailed below (see Fig. 1): 1) type-I impedance $Y^{\mathrm{I}}(s)$ including the impact of IM and RSC; 2) type-II impedance $Y^{\mathrm{II}}(s)$, including the impact of IM,RSC and PLL; 3) type-III impedance $Y^{\mathrm{III}}(s)$, including the impact of IM, RSC, and GSC; 4) type-IV impedance $Y^{\mathrm{IV}}(s)$, including the impact of IM, RSC, GSC, and PLL; 5) type-V impedance $Y^{\mathrm{V}}(s)$, including the impact of IM, RSC, GSC, SRF-PLL, and the outer dc voltage controller. As can be seen, $Y^{\mathrm{V}}(s)$ constitutes the overall *dq* frame impedance model for the DFIGs. As many S2SO coupling phenomena are aroused by the PLL, the different impedances whether considering the PLL or not should be studied. For example, the differences between $Y^{\mathrm{I}}(s)$ / $Y^{\mathrm{III}}(s)$ and $Y^{\mathrm{II}}(s)$ /$Y^{\mathrm{IV}}(s)$ lie in whether the impact of SRF-PLL is considered or not.

A. Type-I $Y_I^{dq}(s)$ Including IM Model and the RSC

1) dq Impedance Model of the IM For an IM, the relationships between the voltages/currents of the respective stator and rotor windings in s domain are described as follows:

$$\begin{bmatrix} \boldsymbol{U_s}(s) \\ \boldsymbol{U_r}(s) \end{bmatrix} = \begin{bmatrix} \boldsymbol{Z}_{ss} & \boldsymbol{Z}_{sr} \\ \boldsymbol{Z}_{rs} & \boldsymbol{Z}_{rr} \end{bmatrix} \begin{bmatrix} \boldsymbol{I_s}(s) \\ \boldsymbol{I_r}(s) \end{bmatrix} \tag{1}$$

where

$$\begin{aligned} Z_{ss} &= \begin{bmatrix} R_s + sL_s & -\omega_1 L_s \\ \omega_1 L_s & R_s + sL_s \end{bmatrix}, Z_{sr} = \begin{bmatrix} sL_m & -\omega_1 L_m \\ \omega_1 L_m & sL_m \end{bmatrix} \\ Z_{rs} &= \begin{bmatrix} sL_m & -\omega_2 L_m \\ \omega_2 L_m & sL_m \end{bmatrix}, Z_{rr} = \begin{bmatrix} R_r + sL_r & -\omega_2 L_r \\ \omega_2 L_r & R_r + sL_r \end{bmatrix} \end{aligned} \tag{2}$$

and $U_s = [U_{sd},\, U_{sq}]^T, I_s = [I_{sd},\, I_{sq}]^T$, $U_r = [U_{rd}, U_{rq}]^T$, $I_r = [I_{rd},\, I_{rq}]^T$, U_{sd} and U_{sq} are, respectively, the d and q components of the stator voltage; U_{rd} and U_{rq} are, respectively, the d and q components of the rotor voltage; I_{sd} and I_{sq} are, respectively, the d and q components of the stator current; and I_{rd} and I_{rq} are, respectively, the d and q components of the rotor current.

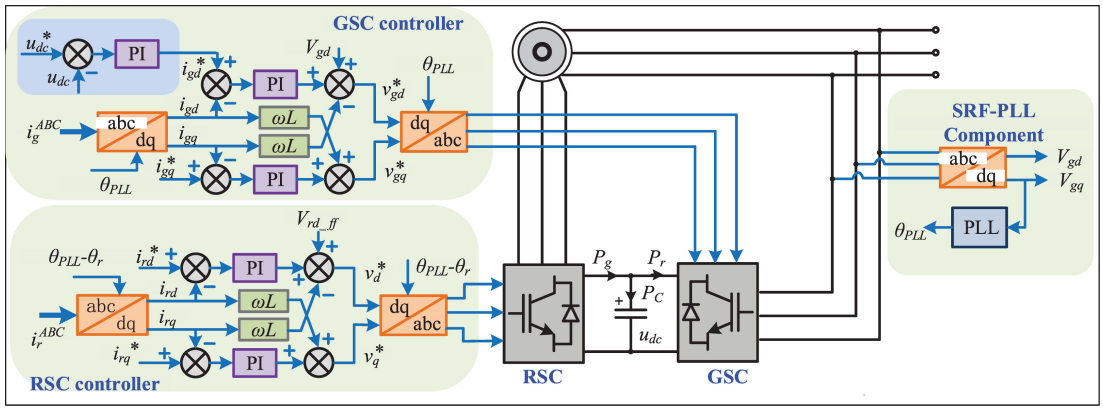

Fig. 1. Topology and the controller of a DFIG.

From (1), the small signal model of an IM is given as follows:

$$\begin{cases} \Delta \boldsymbol{I}_s(s) = \boldsymbol{Y}_{ss}\Delta \boldsymbol{U}_s(s) + \boldsymbol{Y}_{sr}\Delta \boldsymbol{U}_r(s) \\ \Delta \boldsymbol{I}_r(s) = \boldsymbol{G}_{rs}\Delta \boldsymbol{I}_s(s) + \boldsymbol{Y}_{rr}\Delta \boldsymbol{U}_r(s) \end{cases} \tag{3}$$

where

$$\begin{cases} \boldsymbol{Y}_{ss} = \left(\boldsymbol{Z}_{ss} - \boldsymbol{Z}_{sr}\boldsymbol{Z}_{rr}^{-1}\boldsymbol{Z}_{rs}\right)^{-1} \\ \boldsymbol{Y}_{sr} = -\left(\boldsymbol{Z}_{ss} - \boldsymbol{Z}_{sr}\boldsymbol{Z}_{rr}^{-1}\boldsymbol{Z}_{rs}\right)^{-1}\boldsymbol{Z}_{sr}\boldsymbol{Z}_{rr}^{-1} \\ \boldsymbol{G}_{rs} = -\boldsymbol{Z}_{rr}^{-1}\boldsymbol{Z}_{rs} \\ \boldsymbol{Y}_{rr} = \boldsymbol{Z}_{rr}^{-1} \end{cases} \tag{4}$$

2) dq impedance Model of the RSC: As shown in Fig. 1, the dynamic equation of the RSC including the inner current loop is given as follows:

$$\boldsymbol{U}_r(s) = \boldsymbol{Z}_{rPI}\left[\boldsymbol{I}_r^*(s) - \boldsymbol{I}_r(s)\right] + \boldsymbol{Z}_{rX}\boldsymbol{I}_r(s) + \frac{s\boldsymbol{L}_m}{\boldsymbol{L}_s}\boldsymbol{U}_s(s) \tag{5}$$

where

$$\boldsymbol{Z}_{rPI} = \begin{bmatrix} k_{pr} + \frac{k_{ir}}{s} & 0 \\ 0 & k_{pr} + \frac{k_{ir}}{s} \end{bmatrix}, \boldsymbol{Z}_{rX} = \begin{bmatrix} 0 & \omega_2\sigma\boldsymbol{L'}_r \\ -\omega_2\sigma\boldsymbol{L'}_r & 0 \end{bmatrix}, \quad \sigma = 1 - \frac{\boldsymbol{L}_m^2}{\boldsymbol{L}_s\boldsymbol{L'}_r} \tag{6}$$

and $\boldsymbol{I}_r^*(s) = [I_{rd}^*(s) I_{rq}^*(s)]^T$; I_{rd}^* and I_{rq}^* are, respectively, the d and q components of the reference value of the rotor current; s is the slip ratio.

Therefore, when the system voltage is perturbed, the corresponding small signal dynamic equation of the RSC is given as follows:

$$\begin{aligned} \Delta \boldsymbol{U}_r(s) &= \boldsymbol{Z}_{rPI}\left[\Delta \boldsymbol{I}_r^*(s) - \Delta \boldsymbol{I}_r(s)\right] + \boldsymbol{Z}_{rX}\Delta \boldsymbol{I}_r(s) \\ &= \boldsymbol{Z}_{rPI}\Delta \boldsymbol{I}_r^*(s) + \left(\boldsymbol{Z}_{rX} - \boldsymbol{Z}_{rPI}\right)\Delta \boldsymbol{I}_r(s). \end{aligned} \tag{7}$$

3) Type-I dq Impedance Model of DFIG $Y_I^{dq}(s)$: Fig. 2 illustrates the overall transfer function matrix based small signal model of the DFIG $Y_I^{dq}(s)$, including the impact of the IM and the RSC, where $Y_I^{dq}(s)$ is calculated by

$$\begin{aligned} \boldsymbol{Y}_I^{dq}(s) = &\left[\boldsymbol{Y}_{sr}^{-1} - \left(\boldsymbol{Z}_{rX} - \boldsymbol{Z}_{rPI}\right)\left(\boldsymbol{G}_{rs} + \boldsymbol{Y}_{rr}\boldsymbol{Y}_{sr}^{-1}\right)\right]^{-1} \\ &\cdot \left[\boldsymbol{Y}_{sr}^{-1}\boldsymbol{Y}_{ss} - \left(\boldsymbol{Z}_{rX} - \boldsymbol{Z}_{rPI}\right)\boldsymbol{Y}_{rr}\boldsymbol{Y}_{sr}^{-1}\boldsymbol{Y}_{ss}\right]. \end{aligned} \tag{8}$$

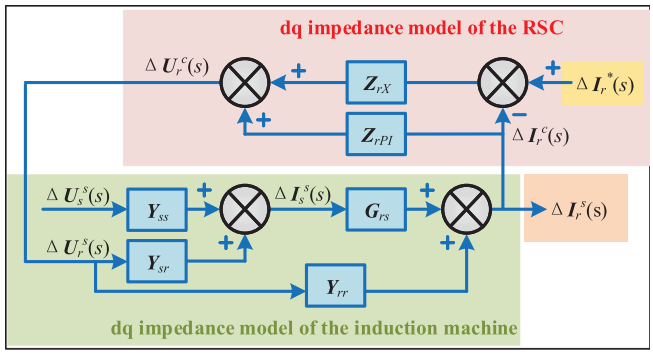

Fig. 2. Type-I $\boldsymbol{Y}_I^{dq}(s)$ including IM model and the RSC.

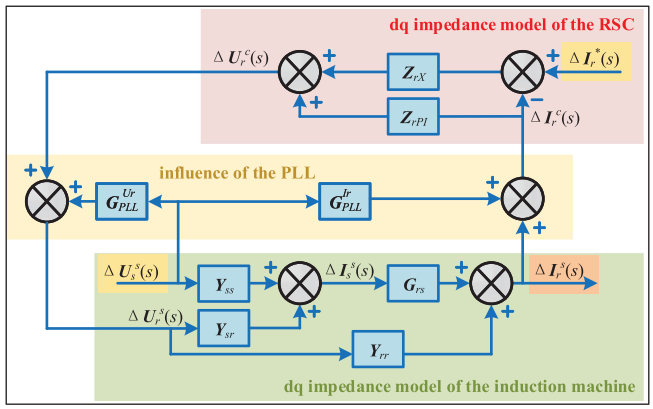

Fig. 3. Type-II $\boldsymbol{Y}_{II}^{dq}(s)$ including IM model, the RSC, and the PLL.

B. Type-II $\boldsymbol{Y}_{II}^{dq}(s)$ Including IM Model, the RSC, and the PLL

Together with the impact of the PLL, the small-signal circuit model Type-II $\boldsymbol{Y}_{II}^{dq}(s)$, including IM model, the RSC, and the PLL can be represented by the transfer function matrix flowchart shown in Fig. 3. As compared from Figs. 2 and 3, small-signal perturbations of the system voltage $\boldsymbol{U}_s$ propagate to the PLL output angle, and further to the values of U_r, I_r, U_g, I_g [16]. This means the impact of the PLL will reshape the final impedance model of the RSC, thus changing the Type-II $\boldsymbol{Y}_{II}^{dq}(s)$.

According to [16], the relationship of $\Delta\theta$ and q component of the stator voltage $\Delta \boldsymbol{U}^s_{sq}(\mathrm{s})$ is

$$\Delta\theta(s) = \frac{H_{\mathrm{PLL}}(s)}{s + U^s_{sd} H_{\mathrm{PLL}}(s)} \Delta \boldsymbol{U}^s_{sq}(\mathrm{s}) = G_{\mathrm{PLL}}(s) \Delta \boldsymbol{U}^s_{sq}(s) \tag{9}$$

where $H_{\mathrm{PLL}}(s) = k_{p_{\mathrm{pll}}} + k_{i_{\mathrm{pll}}}/s$.

Take $\Delta \boldsymbol{U}^s_r$ as an example, the relationship between the measured $\Delta \boldsymbol{U}^c_r$ (affected by the PLL) and the original $\Delta \boldsymbol{U}^s_r$ can be given as follows:

$$\begin{aligned} &\Delta U^c_r(s) + G^{U_r}_{\mathrm{PLL}} \Delta U^s_s(s) = \Delta U^s_r(s) \\ &G^{U_r}_{\mathrm{PLL}} = \begin{bmatrix} 0 & -U^s_{rq}(s) G_{\mathrm{PLL}} \\ 0 & U^s_{rd}(s) G_{\mathrm{PLL}} \end{bmatrix}. \end{aligned} \tag{10}$$

As the reference value of RSC satisfies $\Delta \boldsymbol{I}^*_{\mathrm{r}}(s) = 0$ (see Fig. 3), then the Type-II *dq* impedance can be derived as follows:

$$\begin{aligned} \boldsymbol{Y}^{dq}_{II}(s) = &\left[\boldsymbol{Y}^{-1}_{sr} - (\boldsymbol{Z}_{rX} - \boldsymbol{Z}_{rPI}) \left(\boldsymbol{G}_{rs} + \boldsymbol{Y}_{rr} \boldsymbol{Y}^{-1}_{sr}\right)\right]^{-1} \\ &\begin{bmatrix} \boldsymbol{G}^{I_r}_{\mathrm{PLL}} (\boldsymbol{Z}_{rX} - \boldsymbol{Z}_{rPI}) + \boldsymbol{G}^{U_s}_{\mathrm{PLL}} + \boldsymbol{G}^{\boldsymbol{U}_r}_{\mathrm{PLL}} \\ + \boldsymbol{Y}^{-1}_{sr} \boldsymbol{Y}_{ss} - (\boldsymbol{Z}_{rX} - \boldsymbol{Z}_{rPI}) \boldsymbol{Y}_{rr} \boldsymbol{Y}^{-1}_{sr} \boldsymbol{Y}_{ss} \end{bmatrix}. \end{aligned} \tag{11}$$

C. Type-III $\boldsymbol{Y}^{dq}_{III}(s)$ Including IM Model, the GSC and the RSC

When the impact of the PLL is not considered, the Type-III $\boldsymbol{Y}^{dq}_{\mathrm{III}}(s)$ can be regarded as the Type-I impedance $\boldsymbol{Y}^{dq}_{I}(s)$ in parallel with the impedance of the GSC, or $\boldsymbol{Y}^{dq}_{gI}(s)$.

1) dq Impedance Model of the GSC: As shown in Fig. 1, the relationship between the output voltage of the GSC $\boldsymbol{U}_g$ and the grid voltage $\boldsymbol{U}_s$ satisfies

$$\begin{aligned} &Z_g I_g(s) = U_s(s) - U_g(s) \\ &Z_g = \begin{bmatrix} R_g + sL_g & -\omega_1 L_g \\ \omega_1 L_g & R_g + sL_g \end{bmatrix} \end{aligned} \tag{12}$$

and $U_g(s) = [U_{gd}(s), U_{gq}(s)]^T$ $I_g(s) = [I_{gd}(s), I_{gq}(s)]^T U_{gd}$ and U_{gq} are the d and q components of the output voltage of the GSC; I_{gd} and I_{gq} are the d and q components of the output current of the GSC.

From (12), the small signal model of the GSC is given as follows:

$$\boldsymbol{Z}_g \Delta \boldsymbol{I}_g(s) = \Delta \boldsymbol{U}_s(s) - \Delta \boldsymbol{U}_g(s). \tag{13}$$

As shown in Fig. 1, the dynamic equation of the GSC including the inner current loop is given as follows:

$$\boldsymbol{U}_g(s) = \boldsymbol{Z}_{gPI} \left[\boldsymbol{I}^*_g(s) - \boldsymbol{I}_g(s)\right] + \boldsymbol{Z}_{gX} \boldsymbol{I}_g(s) + \boldsymbol{U}_s(s) \tag{14}$$

where

$$\boldsymbol{Z}_{gPI} = \begin{bmatrix} k_{pg} + \frac{k_{ig}}{s} & 0 \\ 0 & k_{pg} + \frac{k_{ig}}{s} \end{bmatrix}, \boldsymbol{Z}_{gX} = \begin{bmatrix} 0 & \omega_1 L_g \\ -\omega_1 L_g & 0 \end{bmatrix} \tag{15}$$

and $\boldsymbol{I}^*_g(s) = [I^*_{gd}(s),\ I^*_{gq}(s)]^T$, I^*_{gd} and I^*_{gq} denote, respectively, the d and q components of the reference value of the output current of the GSC.

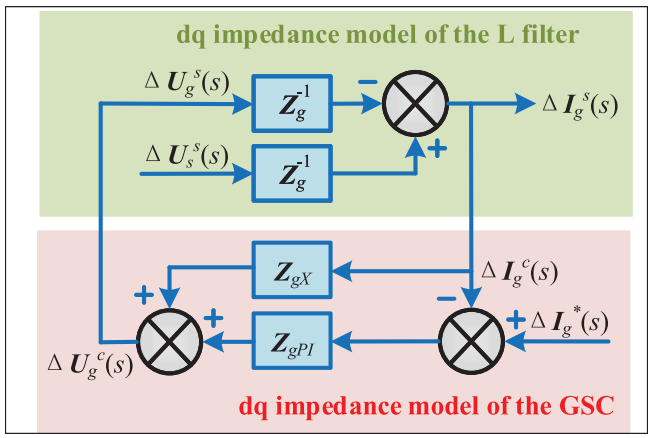

Fig. 4. Type-III impedance model of the GSC $\boldsymbol{Y}^{dq}_{\mathrm{III}}(s)$ (without the impact of the PLL).

Therefore, when the system voltage is perturbed, the overall small signal dynamic equation of the GSC is given as follows:

$$\begin{aligned} \Delta \boldsymbol{U}_g(s) &= \boldsymbol{Z}_{gPI} \left[\Delta \boldsymbol{I}^*_g(s) - \Delta \boldsymbol{I}_g(s)\right] + \boldsymbol{Z}_{gx} \Delta \boldsymbol{I}_g(s) \\ &= \boldsymbol{Z}_{gPI} \Delta \boldsymbol{I}^*_g(s) + (\boldsymbol{Z}_{gx} - \boldsymbol{Z}_{gPI}) \Delta \boldsymbol{I}_g(s). \end{aligned} \tag{16}$$

2) III Type dq Impedance Model of DFIG $\boldsymbol{Y}^{dq}_{III}(s)$: The *dq* impedance model of the GSC is given in Fig. 4, thus the *dq* impedance of the GSC $\boldsymbol{Y}^{dq}_{gI}(s)$ can be obtained as follows:

$$\boldsymbol{Y}^{dq}_{gI}(s) = [\boldsymbol{Z}_g - (\boldsymbol{Z}_{gX} - \boldsymbol{Z}_{gPI})]^{-1}. \tag{17}$$

Finally, combined with the impact of the IM and the RSC (Type-I *dq* impedance), the Type-III *dq* impedance is given by the following:

$$\boldsymbol{Y}^{dq}_{\mathrm{III}}(s) = \boldsymbol{Y}^{dq}_{I}(s) + \boldsymbol{Y}^{dq}_{gI}(s). \tag{18}$$

D. Type-IV $\boldsymbol{Y}^{dq}_{IV}(s)$ Including IM Model, the GSC, the RSC and the PLL

Fig. 5 illustrates the *dq* impedance model of the GSC considering the impact of the PLL, thus the corresponding *dq* impedance of the GSC $\boldsymbol{Y}^{dq}_{gII}(s)$ can be derived as follows:

$$\begin{aligned} \boldsymbol{Y}^{dq}_{gII}(s) = &[\boldsymbol{Z}_g - (\boldsymbol{Z}_{gX} - \boldsymbol{Z}_{gPI})]^{-1} \\ &\left[\boldsymbol{I} + (\boldsymbol{Z}_{gX} - \boldsymbol{Z}_{gPI}) \boldsymbol{G}^{\boldsymbol{I}_g}_{\mathrm{PLL}} - \boldsymbol{G}^{\boldsymbol{U}_g}_{\mathrm{PLL}}\right]. \end{aligned} \tag{19}$$

Combined with the impact of the IM, the RSC, and the PLL (Type-II *dq* impedance), the Type-IV *dq* impedance is given by the following:

$$\boldsymbol{Y}^{dq}_{\mathrm{IV}}(s) = \boldsymbol{Y}^{dq}_{\mathrm{II}}(s) + \boldsymbol{Y}^{dq}_{gII}(s). \tag{20}$$

E. Type-V $\boldsymbol{Y}^{dq}_{V}(s)$ Including the PLL, IM Model, the GSC, the RSC, and the dc Link

Usually, the dc voltage of the capacitor for the back-to-back converter in DFIG will fluctuate when the active powers flowing through the GSC and the RSC are not balanced. In order to maintain the dc voltage of the capacitor, the outer dc voltage controller

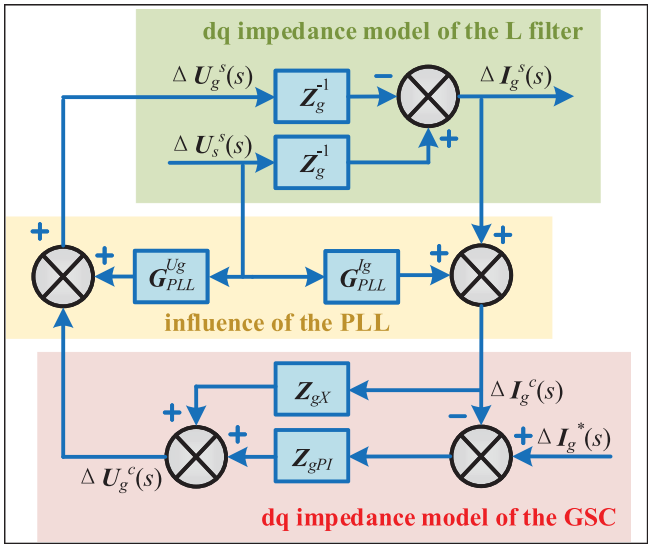

Fig. 5. *dq* impedance model of the GSC considering the impact of the PLL.

can be added. However, when the outer dc voltage controller is considered, the impedance of DFIG (Type-V $\boldsymbol{Y}_V^{dq}(s)$) cannot be regarded as Type-II, including IM model, the RSC, and the PLL, or $\boldsymbol{Y}_{II}^{dq}(s)$ in parallel with the GSC impedance $\boldsymbol{Y}_{gI}^{dq}(s)$.

1) DC Link Between the GSC and the RSC: As shown in Fig. 1, the perturbations of the active powers related to the GSC, the RSC and the dc capacitor satisfy

$$1.5\begin{bmatrix} U_{gd}\Delta I_{gd}(s)+\Delta U_{gq}(s)I_{gq} \\ +U_{gd}\Delta I_{gd}(s)+\Delta U_{gq}(s)I_{gq}\end{bmatrix} -1.5\begin{bmatrix} U_{rd}\Delta I_{rd}(s)+\Delta U_{rq}(s)I_{rq} \\ +U_{rd}\Delta I_{rd}(s)+\Delta U_{rq}(s)I_{rq}\end{bmatrix} = 2sCU_{\rm dc}\Delta U_{\rm dc}. \tag{21}$$

2) dq Impedance Model of the Outer dc Voltage Controller: For the dc voltage controller, the dynamic equation is given as follows:

$$\boldsymbol{I}_{gd}^{*} = \boldsymbol{G}_{{\rm dc}PI}\left[\boldsymbol{U}_{\rm dc}^{*}(s)-\boldsymbol{U}_{\rm dc}(s)\right]. \tag{22}$$

Therefore, when the system voltage is perturbed, the corresponding small signal dynamic equation of the dc link can be obtained as follows:

$$\Delta I_{gd}^{*} = -\Delta U_{\rm dc}(s)G_{{\rm dc}PI}$$
$$G_{{\rm dc}PI} = \begin{bmatrix} k_{pg}+\frac{k_{ig}}{s} & 0 \\ 0 & k_{pg}+\frac{k_{ig}}{s}\end{bmatrix}. \tag{23}$$

The Type V $\boldsymbol{Y}_V^{dq}(s)$ including IM model, the RSC, the GSC, the dc link, and the PLL is shown in Fig. 6, from which the Type-V *dq* impedance $\boldsymbol{Y}_V^{dq}(s)$ can be derived as follows:

$$A = I'_{\rm g}\left(I-G_{\rm pll}^{U_{\rm g}}\right)+U'_{\rm g}G_{\rm pll}^{I_{\rm g}}+I'_{\rm r}\left(G_{\rm sr}^{-1}Y_{\rm ss}+G_{\rm pll}^{U_{\rm r}}\right) -U'_{\rm r}\left(G_{\rm pll}^{I_{\rm r}}-G_{\rm rr}G_{\rm sr}^{-1}Y_{\rm ss}-G_{\rm rr}G_{\rm pll}^{U_{\rm r}}\right) -\left(I'_{\rm r}G_{\rm sr}^{-1}+U'_{\rm r}\left(G_{\rm rs}+G_{\rm rr}G_{\rm sr}^{-1}\right)\right)*Y_{II}^{dq}(s) \tag{24}$$

$$B = -I'_{\rm g}Z_{\rm rX}+U'_{\rm g} \tag{25}$$

$$Y_{gII}^{'dq}(s) = -\left(-Z_{\rm gX}+Z_{\rm gPI}+Z_{\rm g}+\frac{1.5}{sCU_{\rm dc}}Z_{\rm gPI}G_{{\rm dc}PI}B\right)^{-1} \left(G_{\rm pll}^{U_{\rm g}}-I-\left(Z_{\rm gX}-Z_{\rm gPI}\right)G_{\rm pll}^{I_{\rm g}} +\frac{1.5}{sCU_{\rm dc}}Z_{\rm gPI}G_{{\rm dc}PI}A\right) \tag{26}$$

$$Y_V^{dq}(s) = Y_{II}^{dq}(s)+Y_{gII}^{'dq}(s). \tag{27}$$

As can be seen from (27), the Type-V $\boldsymbol{Y}_V^{dq}(s)$ can be regarded as the Type-II impedance $\boldsymbol{Y}_{II}^{dq}(s)$ in parallel with a modified impedance of the GSC, or $Y_{gII}^{'dq}(s)$, where the impact of the PLL is included in $Y_{gII}^{'dq}(s)$.

III. Shifted Frequency Based S2SIM (SF-S2SIM) of DFIGs

Up to now, many types of impedance models of the converter are proposed, such as the *dq* frame impedance model, or the sequence impedance model. Both these impedance models are dedicated to study the small-signal electro-magnetic stability of the converter as well as the large-scale ac grids, or even the frequency couplings. As reported in [10], the practical S2SI phenomena was detected in China Southern Grid, which calls for a new defined sub- and super-synchronous impedance matrix. Although the relationship between the *dq* frame impedance model and the sequence impedance model has very well been studied, the relationships between the *dq* frame impedance model, the sequence impedance model and the sub-/super-synchronous impedance matrix has never been touched before.

As shown in Fig. 7, the relationships between *dq* impedance matrix, the sequence impedance matrix, and the sub-/super-synchronous impedance matrix will be revealed in this section. First, the relationships between *dq* and sequence impedance models are derived the matrix transformation. In other words, the sequence impedance model of DFIGs can be derived by the *dq* impedance model based on either analytical calculations or measurements. Then, the time-domain S2SIM can be derived by frequency shifting of the sequence impedance model. Finally, the more general phasor-domain shifted frequency based S2SIM (SF-S2SIM) of the DFIG is proposed to study the mechanism of the S2SI phenomenon. It should be noted that the proposed S2SIM or SF-S2SIM can be calculated by shifted phasors in phasor domain [26] or by the shifted frequency of different elements for the sequence impedance matrix.

A. Relationship Between dq Impedance and Sequence Impedance

The relationship between voltage and current in the *dq* domain is described as follows:

$$\begin{bmatrix}\Delta \boldsymbol{I}_d(s) \\ \Delta \boldsymbol{I}_q(s)\end{bmatrix} = \begin{bmatrix}\boldsymbol{Y}_{dd}(s) & \boldsymbol{Y}_{dq}(s) \\ \boldsymbol{Y}_{qd}(s) & \boldsymbol{Y}_{qq}(s)\end{bmatrix}\begin{bmatrix}\Delta \boldsymbol{U}_d(s) \\ \Delta \boldsymbol{U}_q(s)\end{bmatrix} \tag{28}$$

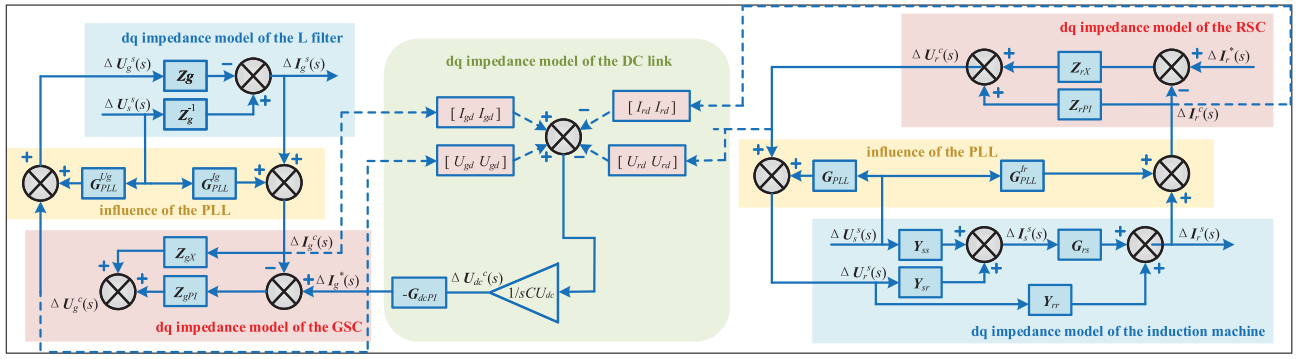

Fig. 6. Type-V $\boldsymbol{Y}_V^{dq}(s)$ including the PLL, IM model, the GSC, the RSC, and the dc link.

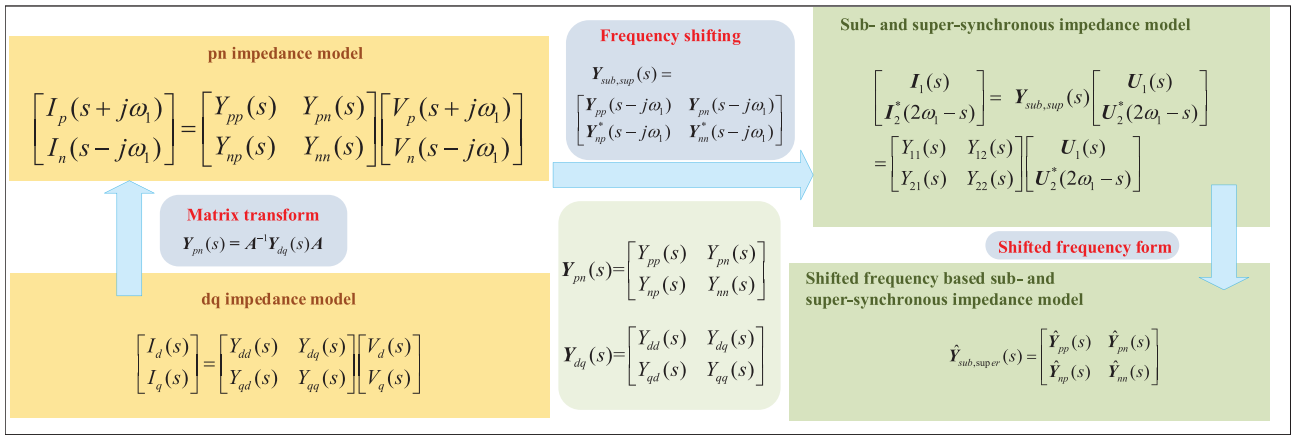

Fig. 7. Relationships between *dq* impedance, sequence impedance, S2SIM, and shifted frequency based S2SIM (SF-S2SIM).

where $\Delta U_d(s)$, $\Delta U_q(s)$, and $\Delta I_d(s)$, $\Delta I_q(s)$ are the voltage and current phasors.

According to the definition of the *pn* impedance, the *pn* impedance matrix can be derived as [24] follows:

$$\boldsymbol{Y}_{pn}(s) = \begin{bmatrix} \boldsymbol{Y}_{+.dq}(s) & \boldsymbol{Y}_{-,dq}(s) \\ \boldsymbol{Y}^*_{-,dq}(s) & \boldsymbol{Y}^*_{+,dq}(s) \end{bmatrix} \tag{29}$$

$$\boldsymbol{Y}^*_{+,dq}(s) = \frac{\boldsymbol{Y}_{dd}(s) + \boldsymbol{Y}_{qq}(s)}{2} - j\frac{\boldsymbol{Y}_{qd}(s) - \boldsymbol{Y}_{dq}(s)}{2}$$

$$\boldsymbol{Y}^*_{-,dq}(s) = \frac{\boldsymbol{Y}_{dd}(s) - \boldsymbol{Y}_{qq}(s)}{2} + j\frac{\boldsymbol{Y}_{qd}(s) + \boldsymbol{Y}_{dq}(s)}{2} \tag{30}$$

where (29) matches the derived results of (31) exactly

$$\boldsymbol{Y}_{pn}(s) = A^{-1}\boldsymbol{Y}_{dq}(s)A,\ A = \begin{bmatrix} 1 & 1 \\ -j & j \end{bmatrix}. \tag{31}$$

B. Time-Domain S2SIM

In order to study S2SI, the relationships between voltage and currents of sub- and super-synchronous frequencies can be modeled as a 2*2 admittance matrix as follows:

$$\begin{bmatrix} I_1(s) \\ I_2^*(2\omega_1 - s) \end{bmatrix} = Y_{\text{sub,sup}}(s) \begin{bmatrix} U_1(s) \\ U_2^*(2\omega_1 - s) \end{bmatrix} = \begin{bmatrix} Y_{11}(s) & Y_{12}(s) \\ Y_{21}(s) & Y_{22}(s) \end{bmatrix} \begin{bmatrix} U_1(s) \\ U_2^*(2\omega_1 - s) \end{bmatrix} \tag{32}$$

where $\boldsymbol{Y}_{\text{sub,super}}(s)$ is defined as the S2SI frequency coupling model of DFIG, in which $Y_{11}(s)$ reflects the influence from voltage perturbation $\boldsymbol{U}_1(s)$ to current response $\boldsymbol{I}_1(s)$; $\boldsymbol{Y}_{12}(s)$ reflects the influence from voltage perturbation $\boldsymbol{U}_2^*(2\omega_1 - s)$ to current response $\boldsymbol{I}_1(s)$; $Y_{21}(s)$ reflects the influence from voltage perturbation $\boldsymbol{U}_1(s)$ to current response $\boldsymbol{I}_2^*(2\omega_1 - s)$; and $Y_{22}(s)$ reflects the influence from voltage perturbation $\boldsymbol{U}_2^*(2\omega_1 - s)$ to current response $\boldsymbol{I}_2^*(2\omega_1 - s)$. The magnitude of these four admittances represents the degree of influence from voltage perturbation to current response, thus the magnitude ratio of the off-diagonal element to the diagonal element can reflect the degree of frequency coupling.

The target of this section is to derive the four elements of the S2SIM based on the elements of the sequence impedance model. For example, in sequence impedance model $\boldsymbol{Y}_{pp}(s)$ is defined as [17] follows:

$$\boldsymbol{Y}_{pp}(s) = \frac{\boldsymbol{I}_p(s + j\omega_1)}{\boldsymbol{U}_p(s + j\omega_1)} \tag{33}$$

where $\boldsymbol{I}_p(s + j\omega_1)$ and $\boldsymbol{U}_p(s + j\omega_1)$ are, respectively, the current and voltage perturbations of the positive sequence.

According to (33), $\boldsymbol{Y}_{11}(s)$ of S2SIM can be derived by frequency shifting of the $\boldsymbol{Y}_{pp}(s)$

$$\boldsymbol{Y}_{11} = \frac{\boldsymbol{I}_1(s)}{\boldsymbol{U}_1(s)} = \boldsymbol{Y}_{pp}(s - j\omega_1). \tag{34}$$

Similarly, the other elements of the S2SIM can be derived as follows:

$$\boldsymbol{Y}_{pn}(s)=\frac{\boldsymbol{I}_p(s+j\omega_1)}{\boldsymbol{U}_n(s-j\omega_1)},\boldsymbol{Y}_{np}(s)=\frac{\boldsymbol{I}_n(s-j\omega_1)}{\boldsymbol{U}_p(s+j\omega_1)}$$

$$\boldsymbol{Y}_{nn}(s)=\frac{\boldsymbol{I}_n(s-j\omega_1)}{\boldsymbol{U}_n(s-j\omega_1)} \tag{35}$$

$$\boldsymbol{Y}_{12}=\frac{\boldsymbol{I}_1(s)}{\boldsymbol{U}_2^*(j2\omega_1-s)}=\boldsymbol{Y}_{pn}(s-j\omega_1) \tag{36}$$

$$\boldsymbol{Y}_{21}=\frac{\boldsymbol{I}_2^*(j2\omega_1-s)}{\boldsymbol{U}_1(s)}=\boldsymbol{Y}_{np}^*(s-j\omega_1) \tag{37}$$

$$\boldsymbol{Y}_{22}=\frac{\boldsymbol{I}_n^*(j2\omega_1-s)}{\boldsymbol{U}_n^*(j2\omega_1-s)}=\boldsymbol{Y}_{nn}^*(s-j\omega_1). \tag{38}$$

Finally, the overall S2SIM of DFIGs can be obtain by frequency shifting of the sequence impedance model $\boldsymbol{Y}_{pn}(s)$

$$\boldsymbol{Y}_{\text{sub,sup}}(s)=\begin{bmatrix}\boldsymbol{Y}_{pp}(s-j\omega_1) & \boldsymbol{Y}_{pn}(s-j\omega_1)\\ \boldsymbol{Y}_{np}^*(s-j\omega_1) & \boldsymbol{Y}_{nn}^*(s-j\omega_1)\end{bmatrix}. \tag{39}$$

C. Phasor-Domain S2SIM

As described in [26] and [27], the whole system incorporating large-scale DFIGs can be modeled in either in time-domain electro-magnetic transient (EMT) models or by shifted phasor domain models. Consequently, the S2SIM can also be derived by shifted phasors of voltage/current perturbations.

A typical signal with the frequency $\omega(s=j\omega)$ can be modeled in the shifted phasor form [27]

$$S(s,t)=\hat{S}(s,t)e^{j\omega_s t}=\hat{S}(s+j\omega_s,t) \tag{40}$$

where $s=j\omega$; $\hat{S}(s,t)$ denotes the shifted phasor of $\boldsymbol{S}(s,t)$; and $\hat{S}(s+j\omega_s,t)$ corresponds to the phasor of $\hat{S}(s,t)$ by right-shifting of 50 Hz.

First, the time-domain perturbations multiplied by $e^{-j\theta}$ can be expressed in the shifted frequency form as

$$\begin{cases}\Delta U(s,t)e^{-j\theta}=\Delta U(s-j\omega_1,t)=\Delta\hat{U}(s,t)\\ \Delta I(s,t)e^{-j\theta}=\Delta I(s-j\omega_1,t)=\Delta\hat{I}(s,t)\end{cases} \tag{41}$$

where $s=j\omega$ represents the frequency of the subsynchronous component; and $\theta=j\omega_1$, where $\omega_1=2\pi f_1=100rad/s$. As is shown, the shifted phasor $\Delta\hat{U}(s,t)$ / $\Delta\hat{I}(s,t)$ can be derived by shifting $\Delta U(s,t)$ / $\Delta I(s,t)$ to the left by 50 Hz.

Based on the concept of shifted frequency phasors, the element of the S2SIM can be derived in the shifted phasor form as follows:

$$\boldsymbol{Y}_{11}=\frac{\boldsymbol{I}_1(s)}{\boldsymbol{U}_1(s)}=\boldsymbol{Y}_{pp}(s-j\omega_1)=\hat{Y}_{pp}(s). \tag{42}$$

Finally, the SF-S2SIM $\hat{Y}_{\text{sub,sup}}(s)$ can be derived by the shifted phasor based sequence impedance model:

$$\hat{Y}_{\text{sub,sup}er}(s)=\begin{bmatrix}\hat{Y}_{pp}(s) & \hat{Y}_{pn}(s)\\ \hat{Y}_{np}(s) & \hat{Y}_{nn}(s)\end{bmatrix} \tag{43}$$

where

$$\hat{Y}_{pn}(s)=\frac{\hat{I}_p(s+j\omega_1)}{\hat{U}_n(s-j\omega_1)}=\frac{\boldsymbol{I}_p(s)}{\boldsymbol{U}_n(s-j2\omega_1)}$$

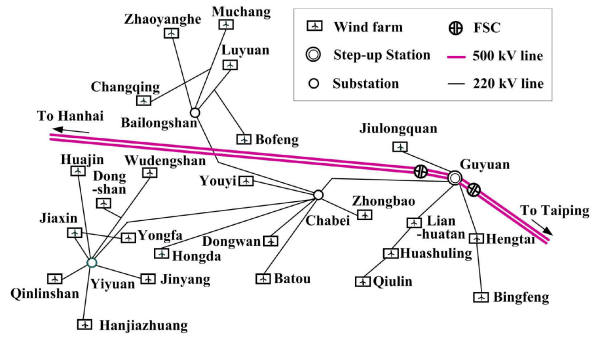

Fig. 8. Single-line diagram of the wind power system in Guyuan area.

$$=\frac{\boldsymbol{I}_p(s)}{\boldsymbol{U}_n^*(j2\omega_1-s)}=\boldsymbol{Y}_{12} \tag{44}$$

$$\hat{Y}_{np}(s)=\frac{\hat{I}_n(s-j\omega_1)}{\hat{U}_p(s+j\omega_1)}=\frac{\hat{I}_n^*(j\omega_1-s)}{\hat{U}_p(s+j\omega_1)}=\frac{\boldsymbol{I}_n^*(j2\omega_1-s)}{\boldsymbol{U}_p(s)}=\boldsymbol{Y}_{21} \tag{45}$$

$$\hat{Y}_{nn}(s)=\frac{\hat{I}_n(s-j\omega_1)}{\hat{U}_n(s-j\omega_1)}=\frac{\boldsymbol{I}_n^*(j2\omega_1-s)}{\boldsymbol{U}_n^*(j2\omega_1-s)}=\boldsymbol{Y}_{22}. \tag{46}$$

IV. Numerical Tests and Validations

A. Description of the Simulated System

The simulated system is the Guyuan area, which is located in the northwest of Hebei Province, China. As show in Fig. 8, it has over 30 wind farms by the end of 2016. All these wind farms distributed throughout the Guyuan area are radially connected to the 220 kV substations of Guyuan, Chabei, Yiyuan and Bailongshan. Then, the electric power is collected at the 500 kV Guyuan substation and next transmitted along two 500 kV corridors, each with double-circuit series-compensated transmission lines, to the North-China power grid.

In the target system, abnormal S2SO events have been observed in recent years. As detailed in [11], the S2SO phenomena will be even more serious for DFIG-based wind farms, such as Hanjiazhuang, or Yongfa wind farms, etc. Typically, the sub- and super-synchronous frequencies of currents are 8.1 and 91.9 Hz, respectively. In order to study, the S2SO phenomena aroused by DFIG-based wind farms, simulation models of the large-scale DFIG-based wind farms as well as the ac grids are set up in PSCAD/EMTDC under a unanimous time-step of 50 μs.

B. Theoretical Calculations and Measurement of (I–V) Type dq Impedance Model for DFIG-Based Wind Farms

In order to compare the differences between the Type I-V DFIG impedance models in an analytical or measurement based way, the magnitude and the angle of *dq* impedance models of DFIG-based wind farms, or the Yongfa wind farms, are depicted in Fig. 9. The comparative analysis of different impedance model of Yongfa wind farm is modeled by 100 same DFIGs, which are connected in parallel. Consequently, the overall impedance

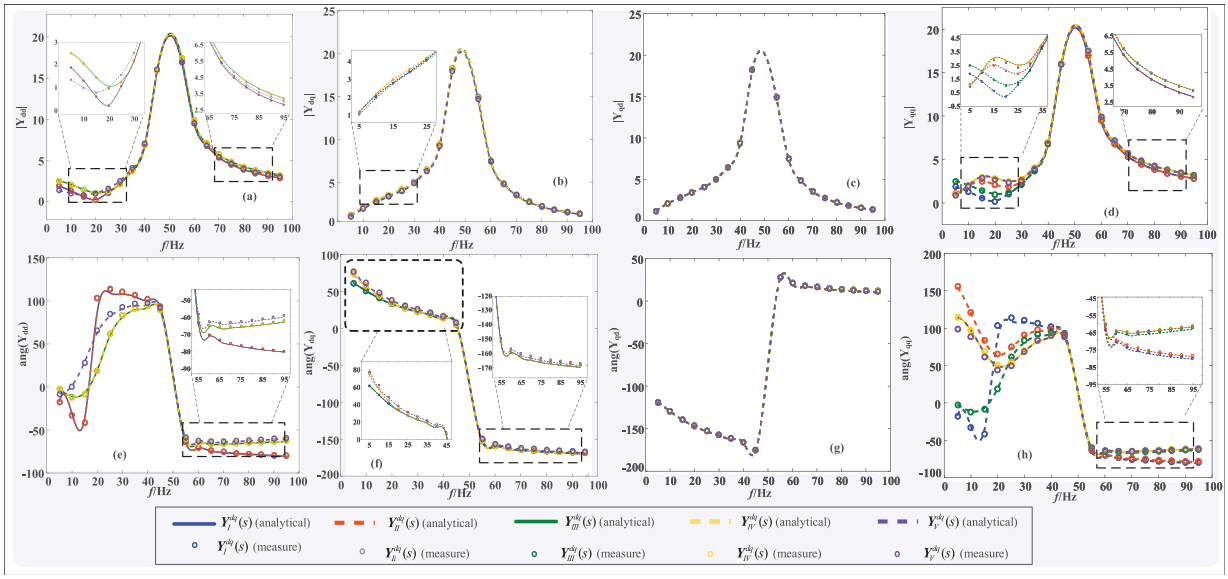

Fig. 9. *dq* impedance model (Type I–V) of the DFIG-based wind farms (measurement and analytical calculation).

model of Yongfa wind farm is similar to one single DFIG, or the impedance of one DFIG is multiplied by a fixed parameter. According to Fig. 9, the following conclusions can be reached. The theoretical quantities of the magnitude and the angle of Y*dq* match very well with those quantities derived by measurement, which verify the effectiveness of Type I–V DFIG *dq* impedance models. The differences between type I–V DFIG *dq* impedance models lie primarily in Y_{dd} and Y_{qq}, especially in subsynchronous frequency band (0–20 Hz) and super-synchronous frequency band (80–100 Hz).

Specifically, $\boldsymbol{Y}_{dd}$ between Type-I/Type-III and Type-II/IV overlaps with each other [see Fig. 9(a) and (e)], indicating that the PLL has little impact on the magnitude of $\boldsymbol{Y}_{dd}$. On the contrary, there are significant gaps between the Type-V *dq* impedance model $\boldsymbol{Y}_V^{dq}(s)$ and the other four impedance models, which shows that the outer dc voltage controller will have a significant impact on the magnitude of $\boldsymbol{Y}_{dd}$.

For $\boldsymbol{Y}_{dq}$ and $\boldsymbol{Y}_{qd}$, as shown in Fig. 9 (b), (c), (f), and (g), the Type I–V *dq* impedance models of the DFIGs are almost overlapped. Noticeably, there are no couplings in *dq* axis when the PLL is not considered. As a result, the $\boldsymbol{Y}_{dq}$ and $\boldsymbol{Y}_{qd}$ of Type-I and Type-II *dq* impedance model are the same according to (21). Further the following conclusions can be derived: the PLL and the outer dc voltage controller both have direct impact on the magnitude of $\boldsymbol{Y}_{dq}$ and $\boldsymbol{Y}_{qd}$, especially in subsynchronous frequency of 0–20 Hz, where the impact of the dc voltage controller is more significant.

For $\boldsymbol{Y}_{qq}$, as shown in Fig. 9 (d) and (g), there is very little difference between the Type-IV and Type-V *dq* impedance model, which indicates that the outer dc voltage controller has little impact on the magnitude of $\boldsymbol{Y}_{qq}$. On the contrary, there are significant differences between $\boldsymbol{Y}_{qq}$ of Type-I and Type-II *dq* impedance model, especially in the range of 5–30 Hz, indicating that the PLL can directly reshape the *dq* impedance model of the RSC. The similar conclusion can also be derived between Type-I and Type-II *dq* impedance model, which means that the PLL will reshape the *dq* impedance model of the GSC as well.

The following conclusion can be reached from Fig. 9 and theoretical derivations in Part II.

1) The Type-III *dq* impedance model $Y_{\mathrm{III}}^{dq}(s)$ without considering the effect of the PLL, can be regarded as the Type-I *dq* impedance model $Y_I^{dq}(s)$ in parallel with the *dq* impedance of the GSC $Y_{gI}^{dq}(s)$.
2) The Type-IV *dq* impedance model $Y_{\mathrm{IV}}^{dq}(s)$ considering the effect of the PLL, can be regarded as the Type-II *dq* impedance model $Y_{\mathrm{II}}^{dq}(s)$ in parallel with the PLL related *dq* impedance of the GSC $Y_{gII}^{dq}(s)$
3) The Type-V $Y_V^{dq}(s)$, or the overall *dq* impedance model considering both the PLL and the outer dc voltage loop, can be regarded as the Type-II impedance $Y_{\mathrm{II}}^{dq}(s)$ in parallel with a modified impedance of the GSC, or $Y_{gII}^{'dq}(s)$, where the impact of the PLL is included in $Y_{gII}^{'dq}(s)$.
4) The effect of the PLL on the overall *dq* impedance model can be evaluated by comparing the differences between $Y_{gI}^{dq}(s)$ and $Y_{gII}^{dq}(s)$.
5) The effect of the outer dc voltage loop on the overall *dq* impedance model can be evaluated by comparing the differences between $Y_{gII}^{dq}(s)$ and$Y_{gII}^{'dq}(s)$.
6) The PLL has little impact on the magnitude of Y_{dd}. On the contrary, the outer dc voltage controller will have a significant impact on the magnitude of Y_{dd}.
7) The PLL and the outer dc voltage controller both have direct impact on the magnitude of Y_{dq} and Y_{qd}, especially in subsynchronous frequency of 0–20 Hz, where the impact of the dc voltage controller is more significant.
8) The outer dc voltage controller has little impact on the magnitude of Y_{qq}. On the contrary, the PLL can directly reshape the *dq* impedance model of the RSC and the GSC as well.

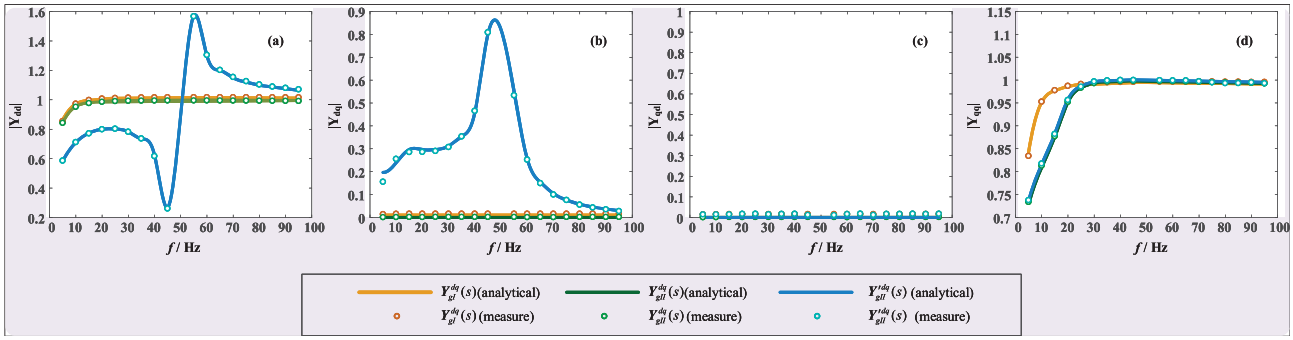

Fig. 10. *dq* impedance model $Y_{gI}^{dq}(s)$, $Y_{gII}^{dq}(s)$, and $Y_{gII}^{'dq}(s)$ of the GSC (measurement and analytical calculation).

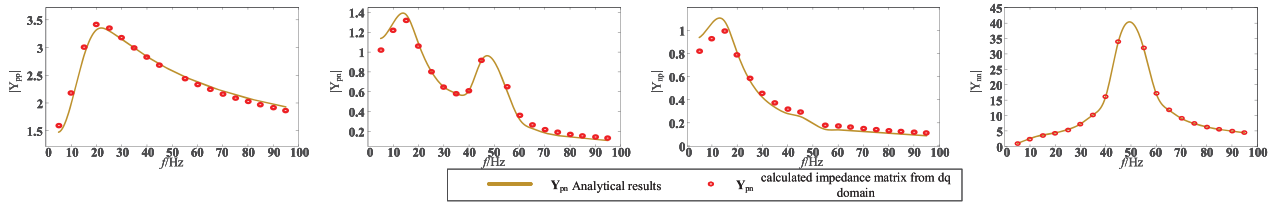

Fig. 11. pn impedance model (V type) of the DFIG-based wind farms (measurement and analytical calculation).

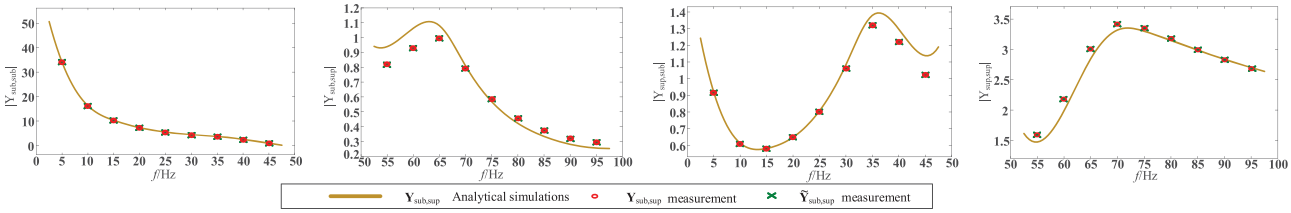

Fig. 12. S2SIM, and SF-S2SIM (V type) of the DFIG-based wind farms (measurement and analytical calculation).

Further, additional conclusions can be reached according to Fig. 10. Comparing the $Y_{gI}^{dq}(s)$ and $Y_{gII}^{dq}(s)$, it is concluded that the bandwidth of the PLL has the direct impact of the low frequency range of Yqq. Comparing the Y_{dq}/Y_{qq} of $Y_{gI}^{dq}(s)/Y_{gII}^{dq}(s)$ and $Y_{gII}^{'dq}(s)$, it is concluded that the *d*- and *q*-axis components are decoupled without considering the impact of the PLL, otherwise components of the *d*- and *q*-axis components are coupled; comparing the $Y_{gII}^{dq}(s)$ and $Y_{gII}^{'dq}(s)$, it is concluded that the impact of the outer dc voltage loop will reshape the value of Y_{dd} and Y_{dq}, resulting in the increase of impedance asymmetry between *d*- and *q*-axis.

C. Relationships Between dq Impedance Model $\boldsymbol{Y}_{dq}(s)$, pn Impedance Model $\boldsymbol{Y}_{pn}(s)$, S2SIM $\boldsymbol{Y}_{\mathrm{sub,super}}(s)$, and the Proposed SF-S2SIM $\hat{Y}_{\mathrm{sub,super}}(s)$

In the following, the Type-V *dq* impedance model is taken as an example to verify the relationships between *dq* impedance model, sequence impedance model, S2SIM, and SF-S2SIM (see Fig. 7).

Fig. 11 compares the measured sequence impedance model Y_{pn} and the calculated impedance matrix from *dq* domain [2], where these results match very well. Fig. 12 compares the analytical results of S2SIM, and the measurement results of S2SIM/SF-S2SIM, where these results are overlapped. Consequently, the following conclusions can be reached: 1) the S2SIM can be derived from frequency shifting of the time-domain sequence impedance model; and 2) the S2SIM can also be derived from shifted phasors of the phasor-domain sequence impedance model.

D. Influencing Factors of Frequency Couplings for the S2SI

In order to study S2SI between the large-scale DFIG-based wind farms and the ac grids, the GNC is used to evaluate the electro-magnetic stability concerning different influence factors, such as parameters of the PLL, the controllers and the SCR of the ac grids [10], etc.

According to the GNC criterion, the $\boldsymbol{L}_{dq}(s)$ matrix of a system constituted by DFIG and a weak grid is defined as follows:

$$L_{dq}(s) = Z_{\mathrm{grid}}^{dq}(s) Y_{V}^{dq}(s)$$
$$Z_{\mathrm{grid}}^{dq} = \begin{bmatrix} R_{\mathrm{grid}} + sL_{\mathrm{grid}} & -\omega_1 L_{\mathrm{grid}} \\ \omega_1 L_{\mathrm{grid}} & R_{\mathrm{grid}} + sL_{\mathrm{grid}} \end{bmatrix} \tag{47}$$

where $\boldsymbol{R}_{\mathrm{grid}}$ and $\boldsymbol{L}_{\mathrm{grid}}$ correspond, respectively, to the Thevenin resistance and inductor of the ac grids. It should be noted

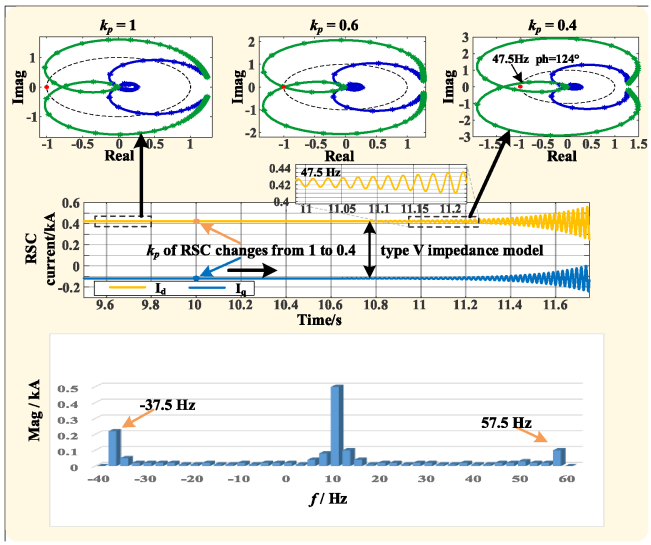

Fig. 13. (a) Loci and time-domain simulation results of S2SIM under different k_p of the GSC. (b) Result of the fast fourier transform (FFT) analysis of the RSC current in abc-axis.

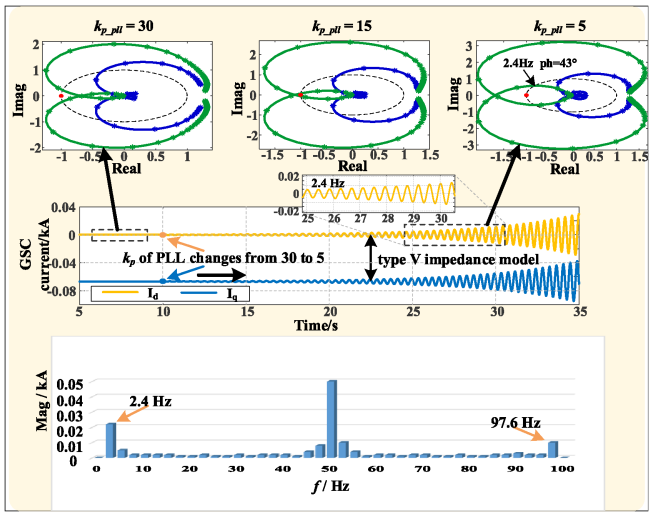

Fig. 14. (a) Loci and time-domain simulation results of S2SIM under different k_p of the PLL. (b) Result of the FFT analysis of the GSC current in abc-axis.

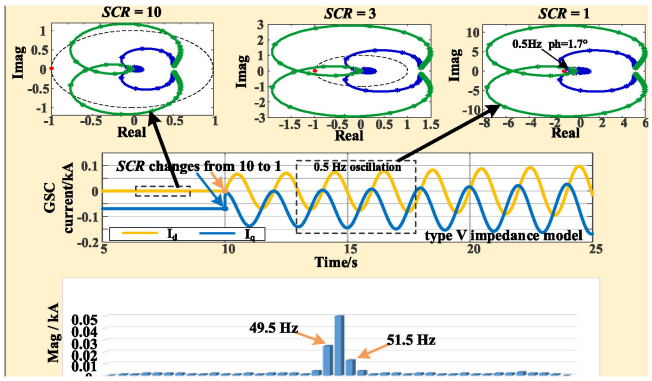

Fig. 15. (a) Loci and time-domain simulation results of S2SIM under different SCR of the ac grids. (b) Result of the FFT analysis of the GSC current in abc-axis.

that if both of the eigenvalue loci of the $\boldsymbol{L}_{dq}(s)$ do not encircle the point of $(-1,\ \mathrm{j}0)$, the system is considered to be stable, otherwise, the system will be unstable. Similar to $\boldsymbol{L}_{dq}(s), \boldsymbol{L}_{pn}(s), \boldsymbol{L}_{\mathrm{sub,super}}(s)$, and $\hat{L}_{\mathrm{sub,super}}(s)$ can be defined as follows:

$$\begin{cases} L_{pn}(s) = Z_{\mathrm{grid}}^{pn}(s) Y_V^{pn}(s) \\ L_{\mathrm{sub,super}}(s) = Z_{\mathrm{grid}}^{\mathrm{sub,super}}(s) Y_V^{\mathrm{sub,super}}(s) \\ \hat{L}_{\mathrm{sub,super}}(s) = \hat{Z}_{\mathrm{grid}}^{\mathrm{sub,super}}(s) \hat{Y}_V^{\mathrm{sub,super}}(s). \end{cases} \tag{48}$$

According to (35), $\boldsymbol{L}_{pn}(s)$ is similar to $\boldsymbol{L}_{dq}(s)$ in s domain, or, $\boldsymbol{L}_{pn}(s) = \boldsymbol{A}^{-1}\boldsymbol{L}_{dq}(s)\boldsymbol{A}$, where they preserve the same eigenvalues. According to Section III, the eigenvalues of S2SIM, SF-S2SIM has a relationship with the sequence impedance model

$$\begin{aligned} \mathrm{eig}\left(\boldsymbol{L}_{pn}(s)\right) &= \mathrm{eig}\left(L_{\mathrm{sub,super}}(s)\right) + j\omega_1 \\ &= \mathrm{eig}\left(\hat{L}_{\mathrm{sub,super}}(s)\right) + j\omega_1. \end{aligned} \tag{49}$$

The electro-magnetic stability of the DFIG farm Yongfa and its associated large-scale ac grids are evaluated based on the S2SIM. Actually, it should be noted that when the SCR is larger than 3.0, or the ac grid is strong, parameters of controllers, including the PLL will have little impact on the overall electro-magnetic stability. On the hand, when the ac grid become weak, the overall electro-magnetic stability will be dramatically influenced by the parameters of controllers. Therefore, the impact of parameters of controllers is evaluated when the SCR of the ac grid is 2.05, which correspond to the practical system in Fig. 8.

1) Influence of K_p for the GSC: Fig. 13 shows the loci and time-domain simulation results of S2SIM under different k_p of the GSC. When $k_p = 1$, no loci encircle the point of $(-1,$ j0), which indicates that the system is stable; when $t = 11\,\mathrm{s}$, or k_p changes to 0.4, the eigenvalue of the loci encircles the point of $(-1,$ j0), indicating that the system is unstable and the time-domain results will produce sustained oscillations of subsynchronous frequency 47.5 Hz. The S2SO frequencies in abc-axis for the RSC is -37.5 and 57.5 Hz, where the sum is 20 Hz. This is because the speed of RSC is 0.8 p.u, and the rated frequency of RSC current in abc axis is 10 Hz.

2) Influence of K_p for the PLL: Fig. 14 shows the loci and time-domain simulation results of S2SIM under different k_p of the PLL. When $k_p = 30\,000$, no loci encircle the point of $(-1,$ j0), which indicates that the system is stable; when $t = 20\,\mathrm{s}$, or kp changes to 5000, the eigenvalue of the loci encircles the point of $(-1,$ j0), indicating that the system is unstable. The oscillation frequency of the loci correspond to the subsynchronous oscillation frequency of the time-domain results, or 2.4 Hz.

3) Influence of SCR for the AC Grids: Fig. 15 shows the loci and time-domain simulation results of S2SIM under different SCR of the ac grids. Before $t = 10\,\mathrm{s}$, the SCR of the ac grid is 10, which produces stable simulation results. Unluckily, when the SCR is decreased to 1.0, the super-low and subsynchronous frequency oscillation at $f = 0.5\,\mathrm{Hz}$ will be produced.

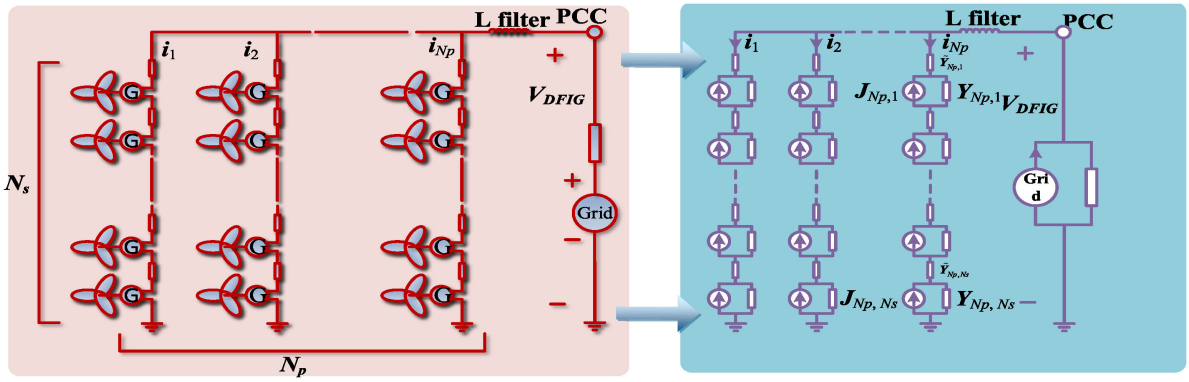

Fig. 16. Topology of a large-scale wind farm and its equivalent circuit.

V. Aggregate S2SIM Model for Large-Scale Wind Farms and Applications of S2SI Analysis

The topology of a typical large-scale wind farm is shown in Fig. 16, DFIGs are integrated to a group by series and paralleled connections, between which are connected by transmission lines, forming the overall the large-scale wind farm. Then, the wind farm is connected to the ac grid at the common coupling (PCC). The electro-magnetic interactions between the wind farm and the grid can be evaluated by the detailed closed-loop impedance characteristics based on the lumped S2SIM models. The lumped S2SIM model of the whole wind farm is established as follows.

In Fig. 16, each DFIG is connected by a transmission line, which can be equivalent to a lumped $R-L$ series model, the dq impedance model of which is given as

$$\tilde{Y}_{i,j}^{\text{sub,sup}}(s)=\begin{bmatrix}\tilde{R}_{i,j}+s\tilde{L}_{i,j} & -\omega_1\tilde{L}_{i,j}\\ \omega_1\tilde{L}_{i,j} & R_{i,j}+s\tilde{L}_{i,j}\end{bmatrix} \tag{51}$$

where $\tilde{R}_{i,j}$ and $\tilde{L}_{i,j}$ are the equivalent lumped resistance and inductance of the transmission line connected to the jth DFIG in the ith group of the wind farm, respectively.

The S2SIM model of the transmission line can be derived as

$$\tilde{Y}_{i,j}^{\text{sub,sup}}(s)=\begin{bmatrix}\tilde{R}_{i,j}+s\tilde{L}_{i,j} & 0\\ 0 & R_{i,j}+s\tilde{L}_{i,j}\end{bmatrix}. \tag{52}$$

Assume that each group consists of N_s DFIGs, and the wind farm is composed by N_p groups (see Fig. 16). Thus, the lumped S2SIM model of the wind farm can be obtained by (50), shown at the bottom of this page, where $Y_f^{\text{sub,sup}}(s)$ is the S2SIM model of the L filter next to the PCC, the derivation of which is similar to $\tilde{Y}_{i,j}^{\text{sub,sup}}(s)$ of (51) and the result is

$$Y_f^{\text{sub,sup}}(s)=\begin{bmatrix}R_f+sL_f & 0\\ 0 & R_f+sL_f\end{bmatrix}. \tag{53}$$

TABLE I
Control Parameters of Different Systems

k_{pr}	0.06	0.06
k_{ir}	1.0	1.0
k_{pg}	1.0	1.0
k_{ig}	20.0	20.0
k_{pdc}	1.0	1.0
k_{idc}	10.0	10.0
k_{p_pll}	1.0	10.0
k_{i_pll}	10.0	100.0

The main control parameters in the DFIG are listed as follows, including the proportional and integral parameters in the PLL, the current controller of the RSC and the GSC, and the dc voltage controller.

$$\begin{cases}k_p=[k_{p\_pll},k_{pr},k_{pg},k_{pdc}\text{pdc}]^T\\ k_i=[k_{i\_pll},k_{ir},k_{ig},k_{idc}]^T.\end{cases} \tag{54}$$

As shown in Fig. 15, low-frequency oscillations in dq domain may occur in the system when the grid is weak. The lumped impedance model of the wind farm of (53) can help further research the effect of the SCR on the interactions between the wind farm and the grid.

Similar to (48), according to the GNC, the $L_{\text{wind}}^{\text{sub,super}}(s)$ of the system composed by a large-scale wind farm and the grid can be obtained by

$$L_{\text{wind}}^{\text{sub,super}}(s)=Z_{\text{grid}}^{\text{sub,super}}(s)Y_{\text{wind}}^{\text{sub,super}}(s). \tag{55}$$

In order to evaluate the effect of the SCR, the operation performances of wind farms with different control parameters can be studied when the SCR changes. The values of the control parameters of the two systems are listed in Table I.

For system I, Fig. 17(a) and (b), respectively, show the eigenvalue loci of the $L_{\text{wind}}^{\text{sub,sup}}(s)$ and the time-domain results of the d and q components of the PCC current when the SCR changes from 1 to 0.8, 0.5, and 0.2. From Fig. 17(b), it can be observed

$$Y_{\text{wind}}^{\text{sub,sup}}(s)=Y_f^{\text{sub,sup}}(s)+\sum_{i=1}^{N_p}\left(\sum_{j=1}^{N_s}\left(\left[Y_{i,j}^{\text{sub,sup}}(s,k_p,k_i)\right]^{-1}+\left[\tilde{Y}_{i,j}^{\text{sub,sup}}(s)\right]^{-1}\right)\right)^{-1} \tag{50}$$

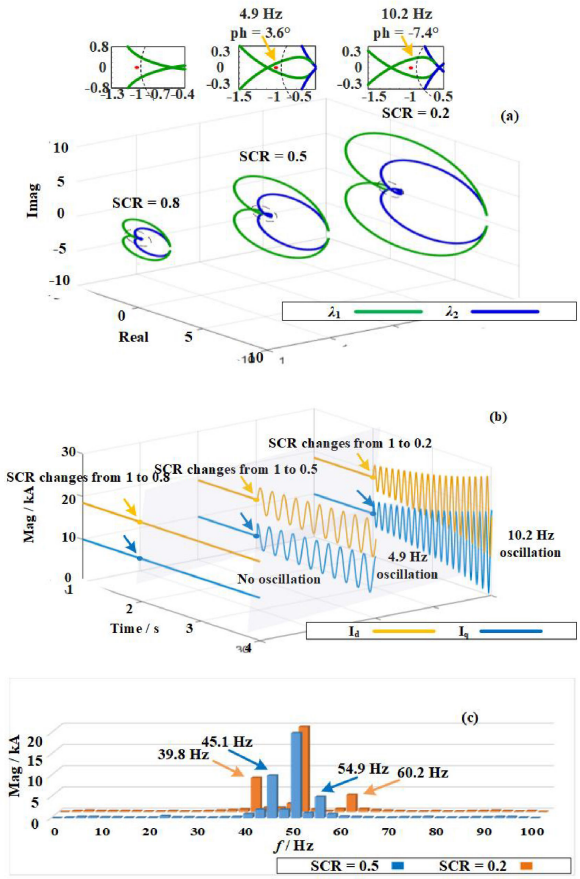

Fig. 17. Simulation results of system I. (a) Eigenvalue loci. (b) Waveforms of the PCC current. (c) Result of FFT analysis.

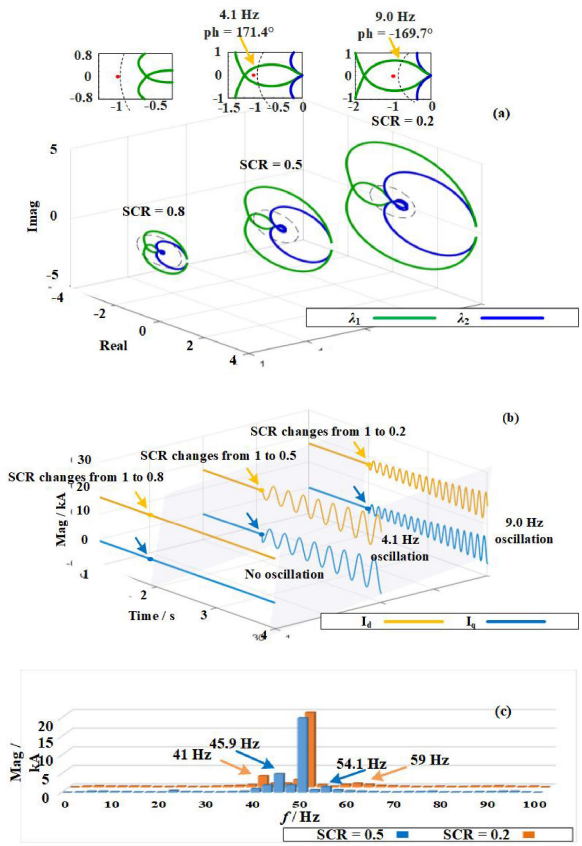

Fig. 18. Simulation results of system II. (a) Eigenvalue loci. (b) Waveforms of the PCC current. (c) Result of FFT analysis.

that when the SCR becomes smaller, i.e., the grid becomes weaker at a particular time, the system may become unstable and oscillation occurs, which verifies the conclusion drawn by Fig. 15. Moreover, when oscillation occurs in the system, the value of SCR can affect the frequency of the oscillation. It can be observed in Fig. 17(c) that the frequency of the subsynchronous component becomes lower when the SCR changes from 0.5 to 0.2. Correspondingly, the oscillation frequency in *dq* -domain will be larger, as shown in Fig. 17(b).

For system II, Fig. 18(a) and (b), respectively, show the eigenvalue loci of the $L_{\text{wind}}^{\text{sub,sup}}(s)$ and the time-domain results of the *d* and *q* components of the PCC current when the SCR changes from 1 to 0.8, 0.5, and 0.2. The similar phenomenon can be observed as system I. As shown in Table. I, the differences between the system I and II are the value of $k_{p_{\text{pll}}}$ and $k_{i_{\text{pll}}}$, which affect the bandwidth of the PLL. The bandwidth of the PLL has a major impact on the stability of the system. If the PLL bandwidth is not wide enough, the PLL will be sensitive to the perturbances in the system and cannot lock the phase to the reference value, which may cause remarkable oscillations with the larger magnitude. According to the transfer function of the PLL, the bandwidth of the PLL of system II is larger than that of system I. As seen in Figs. 18(b) and 17(b), the magnitude of the oscillation of system II is significantly smaller than that of system I. Moreover, as shown in Figs. 18(c) and 17(c), the frequency coupling component of system II is significantly smaller than that of system I, which indicates the remarkable impact of the PLL. It also verifies the conclusion drawn by Fig. 14.

VI. Conclusion

Different from the traditional SSR and SSCI stability issues, the new emerging S2SI related stability issues caused by the interactions of DFIG-based wind farms and the large-scale ac grids have aroused great concerns. For this particular issue, this article is aimed to fill the gap and propose new time-domain and phasor-domain S2SIM, primarily to disclaim the electro-magnetic stability of the S2SI phenomena. Where the relationships between S2SIM/SF-S2SIM and the *dq* /sequence impedance models have been further developed based on matrix transformation and the frequency shifting techniques.

The electro-magnetic stability of the practical DFIG-based wind farms, associated with large-scale ac grids in China has revealed the following.

1) The theoretical derivations of time-domain S2SIM and phasor-domain SF-S2SIM match very well with the measurement results.
2) The correctness of the relationships between the time-domain S2SIM/phasor-domain SF-S2SIM and *dq*/sequence impedance models have been verified by simulation results.

3) The outer dc voltage controller will reshape the*dq* impedance of the DFIGs significantly, especially within the sub- and super-frequency bands; the PLL will have a direct impact on the*dq* impedance model of the sub-frequency band.
4) When the SCR is larger than 3.0, or the ac grid is strong, parameters of controllers, including the PLL will have little impact on the overall electro-magnetic stability. On the hand, when the ac grid become weak, the overall electro-magnetic stability will be dramatically influenced by the parameters of controllers.

REFERENCES

[1] Y. Xu, H. Nian, T. Wang, L. Chen, and T. Zheng, "Frequency coupling characteristic modeling and stability analysis of doubly fed induction generator," *IEEE Trans. Energy Convers.*, vol. 33, no. 3, pp. 1475–1486, Sep. 2018.

[2] C. Zhang, X. Cai, M. Molinas, and A. Rygg, "On the impedance modeling and equivalence of AC/DC side stability analysis of a grid-tied Type IV wind turbine system," *IEEE Trans. Energy Convers.*, vol. 34, no. 2, pp. 1000–1009, Jun. 2019.

[3] D. Wang, L. Liang, J. Hu, N. Chang, and Y. Hou, "Analysis of lowfrequency stability in grid-tied DFIGs by non-minimum phase zero identification," *IEEE Trans. Energy Convers.*, vol. 33, no. 2, pp. 716–729, Jun. 2018.

[4] L. Fan *et al.*, "Modeling of DFIG-based wind farms for SSR analysis," *IEEE Trans. Power Del.*, vol. 25, no. 4, pp. 2073–2082, Oct. 2010.

[5] J. Adams, C. Carter, S. H. Huang, "ERCOT experience with sub-synchronous control interaction and proposed remediation," *IEEE Transmiss. Distrib. Conf. Expo.*, 2012, pp. 1–5.

[6] L. Wang *et al.*, "Investigation of SSR in practical DFIG-based wind farms connected to a series-compensated power system," *IEEE Trans. Power Syst.*, vol. 30, no. 5, pp. 2772–2779, Sep. 2015.

[7] L. P. Kunjumuhammed, B. C. Pal, R. Gupta, and K. J. Dyke, "Stability analysis of a PMSG-based large offshore wind farm connected to a VSCHVDC," *IEEE Trans. Energy Convers.*, vol. 32, no. 3, pp. 1166–1176, Sep. 2017.

[8] W. Ren and E. Larsen, "A refined frequency scan approach to subsynchronous control interaction (SSCI) study of wind farms," *IEEE Trans. Power Syst.*, vol. 31, no. 5, pp. 3904–3912, Sep. 2016.

[9] S. Lamichhane, N. Mithulananthan, "Examination of low-frequency oscillatory stability of power systems with detailed wind farm model," in *Proc. Int. Conf. Power Renew. Energy*, 2017, pp. 121–135.

[10] D. Shu, X. Xie, H. Rao, X. Gao, Q. Jiang, and Y. Huang, "Sub- and supersynchronous interactions between STATCOMs and weak AC/DC transmissions with series compensations," *IEEE Trans. Power Electron.*, vol. 33, no. 9, pp. 7424–7437, Sep. 2018.

[11] X. Xie, X. Zhang, H. K. Liu, H. Liu, Y. Li, and C. Zhang, "Characteristic analysis of subsynchronous resonance in practical wind farms connected to series-compensated transmissions," *IEEE Trans. Energy Convers.*, vol. 32, no. 3, pp. 1117–1126, Sep. 2017.

[12] J. Sun, "Impedance-based stability criterion for grid-connected inverters," *IEEE Trans. Power Electron.*, vol. 26, no. 11, pp. 3075–3078, Nov. 2011.

[13] S. Shah and L. Parsa, "Impedance modeling of three-phase voltage source converters in dq, sequence, and phasor domain," *IEEE Trans. Energy Convers.*, vol. 32, no. 3, pp. 1139–1150, Sep. 2017.

[14] J. Sun, "Small-signal methods for AC distributed power systems–A review," in *Proc. IEEE Elect. Ship Technol. Symp.*, Baltimore, MD, USA, 2009, pp. 44–52.

[15] M. Belkhayat, "Stability criteria for AC power systems with regulated loads,", Ph.D. dissertation, Purdue Univ.,West Lafayette, IN, USA, 1997.

[16] B. Wen *et al.*, "Small signal stability analysis of three-phase AC systems in the presence of constant power loads based on measured d-q frame impedances," *IEEE Trans. Power Electron.*, vol. 30, no. 10, pp. 5952–5963, Oct. 2015.

[17] S. Shah and L. Parsa, "Impedance modeling of three-phase voltage source converters in DQ, sequence, and phasor domains," *IEEE Trans. Energy Convers.*, vol. 32, no. 3, pp. 1139–1150, Sep. 2017.

[18] L. Harnefors, "Modeling of three-phase dynamic systems using complex transfer functions and transfer matrices," *IEEE Trans. Ind. Electron.*, vol. 54, no. 4, pp. 2239–2248, Aug. 2007.

[19] X. Wang, L. Harnefors, F. Blaabjerg, and P. C. Loh, "A unified impedance model of voltage-source converters with phase-locked loop effect," in *Proc. IEEE Energy Convers. Congr. Expo.*, 2016, pp. 1–8.

[20] A. Rygg, M. Molinas, C. Zhang, and X.Cai,"A modified sequence-domain impedance definition and its equivalence to the dq-domain impedance definition for the stability analysis of AC power electronic systems," *IEEE J. Emerg. Sel. Topics Power Electron.*, vol. 4, no. 4, pp. 1383–1396, Dec. 2016.

[21] H. Liu *et al.*, "Subsynchronous interaction between direct-drive PMSG based wind farms and weak AC networks," *IEEE Trans. Power Syst.*, vol. 32, no. 6, pp. 4708–4720, Nov. 20

[22] Z. Miao, "Impedance-model-based SSR analysis for type 3 wind generator and series-compensated network," *IEEE Trans. Energy Convers.*, vol. 27, no. 4, pp. 984–991, Dec. 2012.

[23] Y. Xu *et al.*, "Frequency coupling characteristic modeling of DFIG system based on type-1 frequency-locked loop," *IEEE Energy Convers. Congr. Expo.*, 2018, pp. 942–949

[24] X. Wang, L. Harnefors, and F. Blaabjerg, "Unified impedance model of grid-connected voltage-source converters," *IEEE Trans. Power Electron.*, vol. 33, no. 2, pp. 1775–1787, Feb. 2018.

[25] J. Hu, Q. Hu, B. Wang, H. Tang, and Y. Chi, "Small signal instability of PLL-synchronized type-4 wind turbines connected to high-impedance AC grid during LVRT," *IEEE Trans. Energy Convers.*, vol. 31, no. 4, pp. 1676–1687, Dec. 2016.

[26] D. Shu *et al.*, "A multi-domain co-simulation method for comprehensive shifted-frequency phasor DC-grid models and EMT AC-grid models," *IEEE Trans. Power Electron.*, vol. 34, no. 11, pp. 10557–10574, Feb. 2019.

[27] D. Shu, V. Dinavahi, X. Xie, and Q. Jiang, "Shifted frequency modeling of hybrid modular multilevel converters for simulation of MTDC grid," *IEEE Trans. Power Del.*, vol. 33, no. 3, pp. 1288–1298, Jun. 2018.

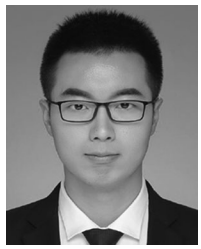

Fan Shi (Student Member, IEEE) received the B.S. degree in electrical engineering from North China Electric Power University, Beijing, China, in 2017. He is currently working toward the M.S. degree with the Department of Electrical Engineering, Shanghai Jiao Tong University, Shanghai, China.

His research interests include modeling, analysis and control of power system with power electronic equipments.

Dewu Shu (Member, IEEE) received the B.Sc. Ph.D. degrees in electrical engineering from Tsinghua University, Beijing, China, in 2013 and 2018, respectively.

He is currently the Tenure-Track Assistant Professor with the Electrical Engineering, Shanghai Jiaotong University. He is an Organizer with the Shanghai Jiatong High Performance Computing Center and the Chair of several conferences such as ECCE, etc. His research interests include high performance computing, VLSI, and 5G techniques.

Zheng Yan (Member, IEEE) received the B.S. degree from Shanghai Jiao Tong University, Shanghai, China, in 1984 and the M.S. and Ph.D. degrees from Tsinghua University, Beijing, China, in 1987 and 1991, respectively, all in electrical engineering.

He is currently a Tenure Professor with the electrical engineering with Shanghai Jiao Tong University. His current research interests include application of optimization theory to power systems, power markets, and dynamic security assessment.

Zhao Song received the B.S. degree in electrical engineering in 2020 from Shanghai Jiao Tong University, Shanghai, China, where he is currently working toward the M.S. degree with the Department of Electrical Engineering.

His research interests include modeling, analysis and control of power system with power electronic equipments.